

Novel oxorhenium(V) complexes of 8-hydroxyquinoline derivatives – Synthesis, spectroscopic characterization, X-ray crystal structures and DFT calculations

B. Machura*, M. Wolff, W. Cieřlik, R. Musiol

Department of Crystallography, Institute of Chemistry, University of Silesia, 9th Szkolna St., 40-006 Katowice, Poland

Department of Organic Chemistry, Institute of Chemistry, University of Silesia, 9th Szkolna St., 40-006 Katowice, Poland

ARTICLE INFO

Article history:

Received 17 October 2012

Accepted 23 December 2012

Available online 17 January 2013

Keywords:

Oxorhenium(V) complexes

8-Hydroxyquinoline

X-ray crystal structure

Electronic structure

DFT and TDDFT calculations

NBO analysis

ABSTRACT

Two modifications of 8-hydroxyquinoline framework, namely 5,7-dichloro-2-[2-(2-chlorophenyl)vinyl]quinoline-8-ol (HL₁) and 2-[2-(3,4-dichlorophenyl)vinyl]quinoline-8-ol (HL₂) have been synthesized and their interaction with [ReOX₃(PPh₃)₂] (X = Cl, Br) have been examined. HL₁ and HL₂ react with [ReOX₃(PPh₃)₂] to give [ReOCl₂(L₁)(PPh₃)₂·MeCN (**1**), [ReOBr₂(L₁)(PPh₃)] (**2**), [ReOCl₂(L₂)(PPh₃)] (**3**) and [ReOBr₂(L₂)(PPh₃)] (**4**). The complexes have been characterized spectroscopically and structurally. The experimental studies on **1** and **3** have been accompanied by DFT calculations, and additional information about binding between the rhenium atom and oxo ligand has been obtained by NBO analysis. The X-ray studies and NBO analysis confirm a triple bond between the rhenium and the terminal oxo ligand. The L₁ and L₂ ligands coordinate in a chelate way via N- and O-donor atoms, and the oxygen donor of the chelate ligand is located *trans* to the terminal oxo (O_t) group due to a strong *trans*-influence of O_t ligand. DFT and TD-DFT calculations applied to **1** and **3** resulted in appropriate prediction of the UV–Vis spectra and enabled a detailed assignment of the electronic transitions to the experimental absorptions.

© 2013 Elsevier Ltd. All rights reserved.

1. Introduction

Compounds containing a quinoline moiety constantly attract the interest of chemist and pharmacist because of their well known and remarkable applications as complexing agents and biological activity [1]. Quinoline is an important heterocyclic contained in various classes of pharmacological agents that can play an important role in biochemical processes [2,3]. A number of compounds incorporating quinoline have been clinically used as antifungal, antibacterial and antiprotozoic drugs [4–7] as well as antituberculous agents [8–10]. Some quinoline analogs showed also antineoplastic activity [11]. Styrylquinolines having therapeutic activity against HIV integrase and FZ41 is an example of such a compound [12].

Since biologically active compounds frequently act *via* chelation, their interaction with metal ions is a subject of considerable interest. The introduction of β[−] emitting isotopes ¹⁸⁶Re (1.07 MeV β-emitter, *t*_{1/2} = 90 h) and ¹⁸⁸Re (2.12 MeV β-emitter, *t*_{1/2} = 17 h) in radiotherapy and success of the ¹⁸⁶Re(Sn)HEDP radiopharmaceutical as a palliative of bone pain has reawakened scientific interest in the coordination chemistry of rhenium. There is a need for new approaches and new labeling procedures. It is

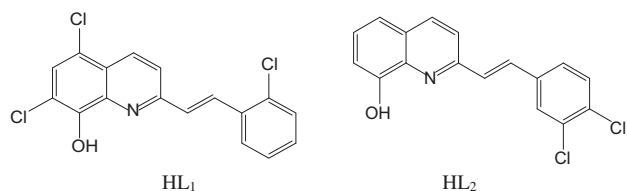
obvious that promising contributions are expected from the coordination chemistry and organometallic chemistry which supplies novel methods and compounds for the radiopharmaceutical community [13–16]. In this context, the design, synthesis and reactivity of the rhenium complexes, especially oxocompounds, has become the aim of several laboratories, including ours.

The main aim of the current study was to obtain chloro substituted derivatives of 2-styrylquinoline and examine their reactivity towards [ReOX₃(PPh₃)₂] (X = Cl, Br). 5,7-Dichloro-2-[2-(2-chlorophenyl)vinyl]quinolin-8-ol (HL₁) was obtained by condensation of 5,7-dichloro-8-hydroxyquinoline with 2-chorobenzaldehyde, whereas 2-[2-(3,4-dichlorophenyl)vinyl]quinoline-8-ol (HL₂) is a product of reaction of 8-hydroxyquinoline with 3,4-dichlorobenzaldehyde in acetic acid anhydride. The compounds differ in number and location of chloro substituents (Scheme 1).

In the next stage, the reactions of 2-styrylquinoline derivatives with [ReOX₃(PPh₃)₂] (X = Cl, Br) were examined and four novel oxocompounds [ReOCl₂(L₁)(PPh₃)₂·MeCN (**1**), [ReOBr₂(L₁)(PPh₃)] (**2**), [ReOCl₂(L₂)(PPh₃)] (**3**) and [ReOBr₂(L₂)(PPh₃)] (**4**) were obtained. To determine molecular structures of the complexes X-ray and spectroscopic (IR, NMR) studies were carried out. Density functional theory (DFT) and time-dependent DFT (TD-DFT) calculations were performed for **1** and **3** to get detailed insight into the electronic structure and spectroscopic properties of the rhenium compounds. Recently, the DFT methods have successfully been applied to study very large systems due to their good compromise

* Corresponding author at: Department of Crystallography, Institute of Chemistry, University of Silesia, 9th Szkolna St., 40-006 Katowice, Poland.

E-mail address: basia@ich.us.edu.pl (B. Machura).



Scheme 1.

between computational cost, coverage, and accuracy of results and have significantly contributed to the characterization of transition metal complexes. Gancheff and co-workers have performed extended tests of the ability of different DFT methods, including B3LYP with LANL2DZ basis set, for rhenium compounds in a geometry optimization and bond nature. Although LANL2DZ is not a very extended basis set, its use with B3LYP has shown to be sufficient for the geometry optimization and calculation of spectral properties. It gives good agreement with the experimental data and its use is justified in the case of large molecules [17].

Additional information about bonding between the rhenium atom and oxo ligand in $[\text{ReOCl}_2(\text{L}_1)(\text{PPh}_3)]$ and $[\text{ReOCl}_2(\text{L}_2)(\text{PPh}_3)]$ has been obtained by NBO analysis [18].

2. Experimental

2.1. General procedure

The $[\text{ReOX}_3(\text{PPh}_3)_2]$ $X = \text{Cl}, \text{Br}$ complexes were prepared according to the literature methods [19]. Styrylquinolines were obtained according to modified literature method [20], and reactions were performed in a laboratory microwave reactor CEM Discovery or on Magnetic stirrer MR Hei-Standard Heidolph. The other reagents used to the synthesis were commercially available and used without further purification. TLC experiments were performed on alumina-backed silica gel 60 F254 plates (Merck, Darmstadt, Germany). The plates were illuminated under UV (254 nm). Melting point was measured on a Thermo-scientific 9100 apparatus. IR spectra were recorded on a Nicolet Magna 560 spectrophotometer in the spectral range $4000\text{--}400\text{ cm}^{-1}$ with the samples in the form of KBr pellets. Electronic spectra were measured on a spectrophotometer Lab Alliance UV-Vis 8500 in the range $1100\text{--}180\text{ nm}$ in methanol solution. ^1H NMR spectra were recorded on a Bruker AM-500 (500 MHz for ^1H), and ^{13}C NMR spectra were recorded on a Bruker AM-400 (100 MHz) instrument (Bruker Bio-Spin Corp., Germany). Chemical shifts are reported in ppm (d) with reference to internal $\text{Si}(\text{CH}_3)_4$, when diffused easily exchangeable signals are omitted. MS spectra were obtained on a mass spectrometer Varian HPLC MS (ESI).

2.2. Preparation of 5,7-dichloro-2-[2-(2-chlorophenyl)vinyl]quinoline-8-ol (HL₁)

5,7-Dichloro-8-hydroxyquinaldine (1.0 mmol) was mixed thoroughly with 4 equiv. of 2-chlorobenzaldehyde, put in an open vessel and exposed to microwave irradiation for 10 min. at $180\text{ }^\circ\text{C}$ and 50 W. The reaction mixture was cool down to $0\text{ }^\circ\text{C}$, and the precipitate was filtered off. The solid was crystallized from ethanol. It gave beige crystals. Yield: 47%, m.p. $205\text{--}210\text{ }^\circ\text{C}$. $m/z = 348.27$ $[\text{M}]^-$; HPLC purity 98.74%; UV (nm), $\lambda_{\text{max}}/\log \epsilon$: 319.9/3.61. ^1H NMR (400 MHz, DMSO- d_6): $\delta = 8.48$ (d, $J = 8.7\text{ Hz}$, 1 H); 8.36 (d, $J = 16.2\text{ Hz}$, 1 H); 7.98 (d, $J = 8.8\text{ Hz}$, 1 H); 7.94 (dd, $J = 7.6, 2.0\text{ Hz}$, 1 H); 7.77 (s, 1 H); 7.58–7.50 (m, 2 H); 7.47–7.36 (m, 2 H) ppm. ^{13}C NMR (100 MHz, DMSO- d_6): $\delta = 155.17, 149.33, 139.39,$

134.81, 133.99, 133.57, 132.06, 131.14, 130.83, 130.44, 128.27, 128.17, 127.85, 124.37, 123.01, 119.63, 116.28 ppm.

2.3. Preparation of 2-[2-(3,4-dichlorophenyl)vinyl]quinoline-8-ol (HL₂)

To a solution of 8-hydroxyquinaldine (2.5 mmol) in acetic anhydride (10 ml) was added 2 equiv. of 3,4-dichlorobenzaldehyde. The mixture was heated and stirred under inert gas atmosphere (N_2) during 20 h at $120\text{ }^\circ\text{C}$, and then it was cooled down to $0\text{ }^\circ\text{C}$, and the precipitate was filtered off. The solid was crystallized from ethanol. It gave yellow crystals. Yield: 96.9%, m.p. $140\text{ }^\circ\text{C}$, $m/z = 317.32$ $[\text{M}+2\text{H}]^+$; HPLC purity 98.48%; UV (nm), $\lambda_{\text{max}}/\log \epsilon$: 293.7/3.53. ^1H NMR (400 MHz, DMSO- d_6): $\delta = 8.44$ (d, $J = 8.6\text{ Hz}$, 1 H), 8.07 (d, $J = 1.7\text{ Hz}$, 1 H), 7.87 (d, $J = 8.5\text{ Hz}$, 2 H), 7.82–7.73 (m, 2 H), 7.70 (d, $J = 8.4\text{ Hz}$, 1 H), 7.59 (d, $J = 6.5\text{ Hz}$, 1 H), 7.58–7.51 (m, 2 H). ^{13}C NMR (100 MHz, DMSO- d_6): $\delta = 169.87, 155.25, 147.59, 140.85, 137.47, 137.31, 132.35, 132.17, 131.36, 131.22, 129.42, 128.80, 127.89, 126.65, 126.12, 122.28, 121.39.$

2.4. Preparation of $[\text{ReOCl}_2(\text{L}_1)(\text{PPh}_3)]_2\text{MeCN}$ (1)

A mixture of $[\text{ReOCl}_3(\text{PPh}_3)_2]$ (0.50 g, 0.60 mmol) and HL₁ (0.23 g, 0.66 mmol) was refluxed in acetonitrile (80 ml) for 6 h. The resulting red-brown solution was left to slow evaporation and dark red crystals were obtained after few days. Yield 70%.

Anal. Calc. $\text{C}_{72}\text{H}_{51}\text{N}_3\text{O}_4\text{Cl}_{10}\text{P}_2\text{Re}_2$: C, 47.75; H, 2.84; N, 2.32. Found: C, 47.63; H, 2.90; N, 2.28%. IR (KBr): 1625(m), 1591(m), 1548(m) $\nu(\text{C}=\text{N})$ and $\nu(\text{C}=\text{C})$; 974(s) cm^{-1} $\nu(\text{Re}=\text{O})$. ^1H NMR (400 MHz, DMSO- d_6): $\delta = 8.51$ (d, $J = 8.6\text{ Hz}$, 1 H); 8.38 (d, $J = 16.1\text{ Hz}$, 1 H); 8.01 (t, $J = 8.04\text{ Hz}$, 1 H); 7.95 (d, $J = 8.2\text{ Hz}$, 1 H); 7.78 (s, 1 H), 7.65–7.53 (m, 17 H), 7.45–7.37 (m, 2 H) ppm.

2.5. Preparation of $[\text{ReOBr}_2(\text{L}_1)(\text{PPh}_3)]$ (2)

A procedure similar to that for **1** was used with $[\text{ReOBr}_3(\text{PPh}_3)_2]$ (0.50 g, 0.52 mmol) and HL₁ (0.198 g, 0.57 mmol). Crystalline precipitate of **2** was collected in 63% yield.

Anal. Calc. $\text{C}_{35}\text{H}_{24}\text{NO}_2\text{P}_2\text{Cl}_3\text{Br}_2\text{Re}$: C, 43.16; H, 2.48; N, 1.44. Found: C, 42.98; H, 2.56; N, 1.32%. IR (KBr): ν/cm^{-1} : IR (KBr): 1626(m), 1593(m), 1549(m) $\nu(\text{C}=\text{N})$ and $\nu(\text{C}=\text{C})$; 972(s) cm^{-1} $\nu(\text{Re}=\text{O})$. ^1H NMR (400 MHz, DMSO- d_6): $\delta = 8.52$ (d, $J = 8.8\text{ Hz}$, 1 H); 8.37 (d, $J = 16.1\text{ Hz}$, 1 H); 8.00 (d, $J = 8.8\text{ Hz}$, 1 H); 7.95 (d, $J = 6.5\text{ Hz}$, 1 H); 7.78 (s, 1 H); 7.65–7.53 (m, 17 H), 7.48–7.39 (m, 2 H) ppm. UV-Vis (CH_3OH ; λ_{max} [nm] (ϵ ; $[\text{dm}^3\text{ mol}^{-1}\text{ cm}^{-1}]$): 672.2 (670); 443.6 (2750); 317.4 (21380); 208 (69550).

2.6. Preparation of $[\text{ReOCl}_2(\text{L}_2)(\text{PPh}_3)]$ (3)

A procedure similar to that for **1** was used with $[\text{ReOCl}_3(\text{PPh}_3)_2]$ (0.50 g, 0.60 mmol) and HL₂ (0.21 g, 0.66 mmol). Crystalline precipitate of **3** was collected in 74% yield.

Anal. Calc. $\text{C}_{35}\text{H}_{25}\text{Cl}_4\text{NO}_2\text{PRe}$: C, 49.42; H, 2.96; N, 1.65%. Found: C, 49.32; H, 2.99; N, 1.71%. IR (KBr): 1626(m), 1601(m), 1558(s) $\nu(\text{C}=\text{N})$ and $\nu(\text{C}=\text{C})$; 965(s) cm^{-1} $\nu(\text{Re}=\text{O})$. ^1H NMR (400 MHz, DMSO- d_6): $\delta = 8.19$ (d, $J = 2.2\text{ Hz}$, 2 H), 7.74 (d, $J = 8.3\text{ Hz}$, 1H), 7.71 (s, 1H), 7.67–7.59 (m, 2H), 7.57–7.53 (m, 2H), 7.51–7.40 (m, 2H), 7.37–7.29 (m, 8H), 7.28–7.19 (m, 7H) ppm.

2.7. Preparation of $[\text{ReOBr}_2(\text{L}_2)(\text{PPh}_3)]$ (4)

A procedure similar to that for $[\text{ReOCl}_2(\text{L}_1)(\text{PPh}_3)_2]$ was used with $[\text{ReOBr}_3(\text{PPh}_3)_2]$ (0.50 g, 0.52 mmol) and HL₂ (0.18 g, 0.57 mmol). Crystalline precipitate of **4** was collected in 69% yield.

Anal. Calc. $\text{C}_{35}\text{H}_{25}\text{Br}_2\text{Cl}_2\text{NO}_2\text{PRe}$: C, 48.40; H, 2.90; N, 1.61%. Found: C, 48.27; H, 2.95; N, 1.65%. IR (KBr): 1627(m), 1555(m)

$\nu(\text{C}=\text{N})$ and $\nu(\text{C}=\text{C})$; 968(s) cm^{-1} $\nu(\text{Re}=\text{O})$. ^1H NMR (400 MHz, DMSO- d_6): δ = 8.22 (d, J = 3.2 Hz, 2H), 7.74 (d, J = 2.1 Hz, 1 H), 7.70 (d, J = 1.9 Hz, 1 H), 7.66–7.60 (m, 2H), 7.58–7.53 (m, 2H), 7.46–7.42 (m, 2H), 7.37–7.29 (m, 8H), 7.27–7.20 (m, 7H) ppm. UV–Vis (CH₃OH; λ_{max} [nm] (ϵ ; [$\text{dm}^3 \text{mol}^{-1} \text{cm}^{-1}$])): 658.2 (310); 434.0 (795); 343.8 (7190); 303.8 (9450); 207.0 (27 490).

2.8. Crystal structure determination and refinement

The X-ray intensity data of **1–4** were collected on a Gemini A Ultra diffractometer equipped with Atlas CCD detector and graphite monochromated Mo K α radiation (λ = 0.71073 Å) at room temperature. Details concerning crystal data and refinement are given in Table 1. Lorentz, polarization and empirical absorption correction using spherical harmonics implemented in SCALE3 ABSPACK scaling algorithm [21] were applied. The structures were solved by the Patterson method and subsequently completed by the difference Fourier recycling. All the non-hydrogen atoms were refined anisotropically using full-matrix, least-squares technique. The hydrogen atoms were treated as riding on their parent carbon atoms and assigned isotropic temperature factors equal 1.2 (non-methyl) times the value of equivalent temperature factor of the parent atom. SHELXS97 and SHELXL97 [22,23] programs were used for all the calculations. Atomic scattering factors were those incorporated in the computer programs.

2.9. Computational details

The GAUSSIAN-09 program package was used for all the calculations [24]. The gas phase geometries of [ReOCl₂(L₁)(PPh₃)] and [ReOCl₂(L₂)(PPh₃)] were fully optimized without any symmetry restrictions in singlet ground-states with the DFT method using

the B3LYP hybrid exchange–correlation functional [25,26]. The calculations were performed using ECP LANL2DZ basis set with additional d (with exponent α = 0.3811) and f (with exponent α = 2.033) functions for the rhenium and the standard 6-31G basis set for the other atoms. For chlorine, oxygen and nitrogen atoms, diffuse and polarization functions were added [27–29]. All the calculated vibrational frequencies are real and positive, indicating that the optimized structure represents real minima of the ground state potential energy surface.

The electronic spectra of [ReOCl₂(L₁)(PPh₃)] and [ReOCl₂(L₂)(PPh₃)] were calculated with the TDDFT method and the solvent effect (methanol) was simulated using the polarizable continuum model (PCM) [30]. For both complexes, 120 singlet–singlet spin-allowed excitations in solution were taken into account.

Natural bond orbital (NBO) calculations were performed with the NBO code [31] included in GAUSSIAN-09. Each natural bond orbital (NBO) σ_{AB} can be written in terms of two directed valence hybrids (NHOs) h_A and h_B on atoms A and B:

$$\alpha_{AB} = c_A h_A + c_B h_B$$

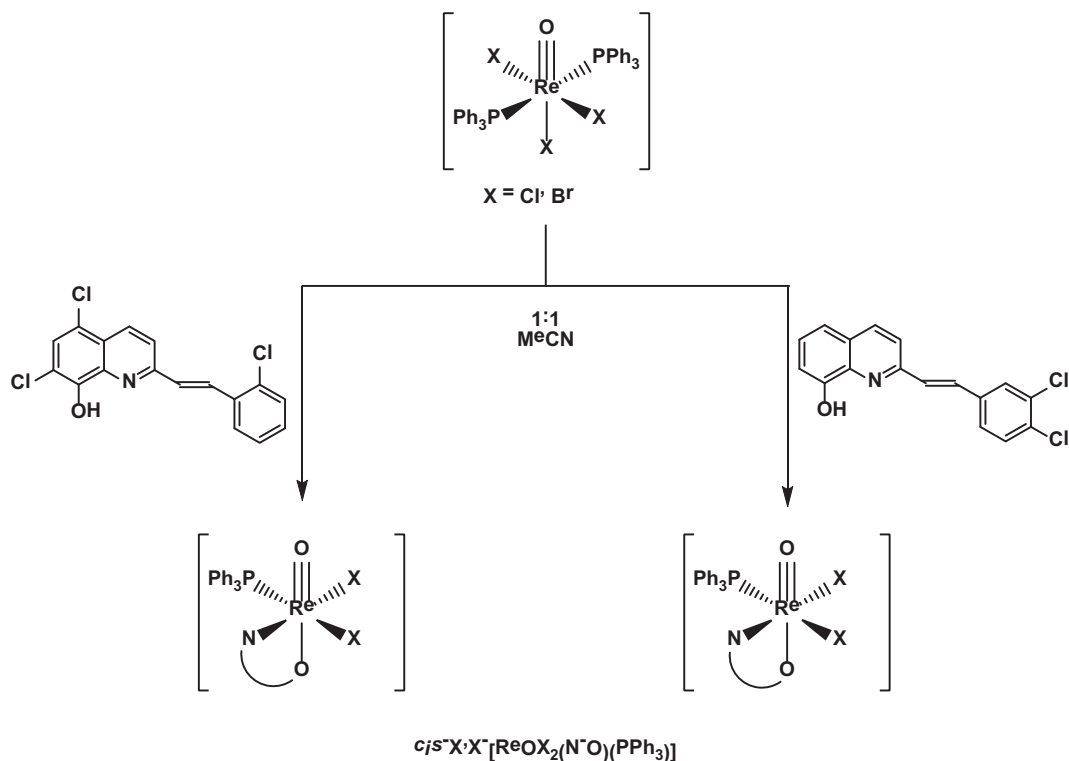
where σ_A and σ_B are polarization coefficients. Each valence bonding NBO must in turn be paired with a corresponding valence antibonding NBO:

$$\alpha_{AB}^* = c_B h_A + c_A h_B$$

to complete the span of the valence space. The Lewis-type (donor) NBOs are thereby complemented by the non-Lewis-type (acceptor) NBOs that are formally empty in an idealized Lewis picture. The interactions between filled (donor) Lewis-type NBOs and empty (acceptor) non-Lewis NBOs lead to loss of occupancy from the localized NBOs of the idealized Lewis structure into the empty non-Lewis orbitals, and they are referred to as ‘delocalization

Table 1
Crystal data and structure refinement for **1**, **2**, **3** and **4**.

	1	2	3	4
Empirical formula	C ₇₂ H ₅₁ N ₃ O ₄ Cl ₁₀ P ₂ Re ₂	C ₃₅ H ₂₄ NO ₂ PCl ₃ Br ₂ Re	C ₃₅ H ₂₅ Cl ₄ NO ₂ PRe	C ₃₅ H ₂₅ Br ₂ Cl ₂ NO ₂ PRe
Formula weight	1811.00	973.89	850.53	939.45
<i>T</i> (K)	295.0(2)	295.0(2)	295.0(2)	295.0(2)
λ (Å)	0.71073	0.71073	0.71073	0.71073
Crystal system	triclinic	orthorhombic	triclinic	monoclinic
Space group	$P\bar{1}$	<i>Pbca</i>	$P\bar{1}$	<i>P21/c</i>
<i>Unit cell dimensions</i>				
<i>a</i> (Å)	10.6143(3)	15.8184(3)	10.4506(3)	11.2274(4)
<i>b</i> (Å)	15.4252(4)	20.1611(6)	11.5613(4)	18.9869(5)
<i>c</i> (Å)	22.7233(6)	21.2396(5)	15.3803(6)	15.9416(4)
α (°)	74.071(2)		75.742(3)	90
β (°)	77.602(2)		87.451(3)	102.878(3)
γ (°)	84.069(2)		65.974(3)	90
<i>V</i> (Å ³)	3490.24(16)	6773.7(3)	1641.73(10)	3312.87(18)
<i>Z</i>	2	8	2	4
<i>D</i> _{calc} (Mg/m ³)	1.723	1.910	1.721	1.884
Absorption coefficient (mm ^{−1})	3.945	6.265	4.108	6.323
<i>F</i> (000)	1772	3744	832	1808
Crystal size (mm)	0.180 × 0.110 × 0.016	0.302 × 0.152 × 0.015	0.156 × 0.072 × 0.028	0.160 × 0.082 × 0.038
θ (°)	3.41–25.00	3.37–25.00	3.37–25.00	3.39–25.00
Index ranges	−12 ≤ <i>h</i> ≤ 12, −18 ≤ <i>k</i> ≤ 18 −27 ≤ <i>l</i> ≤ 24	−18 ≤ <i>h</i> ≤ 18 −23 ≤ <i>k</i> ≤ 23 −25 ≤ <i>l</i> ≤ 25	−12 ≤ <i>h</i> ≤ 12 −13 ≤ <i>k</i> ≤ 13 −18 ≤ <i>l</i> ≤ 18	−12 ≤ <i>h</i> ≤ 13 −22 ≤ <i>k</i> ≤ 22 −18 ≤ <i>l</i> ≤ 16
Reflections collected	33647	50407	17258	16033
Independent reflections (<i>R</i> _{int})	12281 (0.0559)	5947 (0.0903)	5772 (0.0373)	5820 (0.0566)
Completeness to 2 θ = 25.00°	99.7%	99.7%	99.8%	99.7%
Minimum and maximum transmission	0.616–1.000	0.375–1.000	0.700–1.000	0.352–1.000
Data/restraints/parameters	12270/0/839	5947/0/406	5772/0/397	5820/0/397
Goodness-of-fit (GOF) on <i>F</i> ²	0.936	1.059	1.053	0.927
Final <i>R</i> indices [<i>I</i> > 2 σ (<i>I</i>)]	<i>R</i> ₁ = 0.0334 <i>wR</i> ₂ = 0.0538	<i>R</i> ₁ = 0.0357 <i>wR</i> ₂ = 0.0827	<i>R</i> ₁ = 0.0240 <i>wR</i> ₂ = 0.0562	<i>R</i> ₁ = 0.0457 <i>wR</i> ₂ = 0.0974
<i>R</i> indices (all data)	<i>R</i> ₁ = 0.0570 <i>wR</i> ₂ = 0.0581	<i>R</i> ₁ = 0.0517 <i>wR</i> ₂ = 0.0895	<i>R</i> ₁ = 0.0293 <i>wR</i> ₂ = 0.0580	<i>R</i> ₁ = 0.0826 <i>wR</i> ₂ = 0.1079
Largest difference peak and hole (e Å ^{−3})	0.773 and −0.730	1.077 and −0.982	0.899 and −0.621	1.423 and −1.182



Scheme 2. Formation of $[\text{ReO}_x\text{X}_2(\text{L}_1)(\text{PPh}_3)]$ and $[\text{ReO}_x\text{X}_2(\text{L}_2)(\text{PPh}_3)]$ complexes in the reactions of $[\text{ReO}_3(\text{PPh}_3)_2]$ with a suitable ligand HL_1 or HL_2 .

corrections to the zeroth-order natural Lewis structure. The stabilization energy ΔE_{ij} (kcal/mol) associated with delocalization is estimated by the second-order perturbative as

$$\Delta E_{ij} = q_i(F(i,j)^2)/(\varepsilon_i - \varepsilon_j)$$

where q_i is the donor orbital occupancy, ε_i , ε_j are diagonal elements (orbital energies) and $F(i,j)$ is the off-diagonal NBO Fock or Kohn-Sham matrix element [18].

Table 2
Hydrogen bonds for **1**, **2**, **3** and **4**.

D	A	D–H (Å)	H···A (Å)	D···A (Å)	D–H···A (°)
1					
C(2)–H(2)···Cl(1)		0.93	2.78	3.623(5)	151.9
C(12)–H(12)···O(2)		0.93	2.50	3.124(6)	124.8
C(25)–H(25)···Cl(4)		0.93	2.76	3.109(5)	103.4
C(28)–H(28)···O(1)		0.93	2.40	2.794(5)	105.3
C(29)–H(29)···Cl(5)		0.93	2.72	3.051(5)	102.0
C(29)–H(29)···Cl(6)_#1		0.93	2.81	3.724(4)	169.1
C(38)–H(38)···Cl(1)_#2		0.93	2.79	3.486(6)	132.2
C(47)–H(47)···O(4)		0.93	2.27	3.071(6)	143.5
C(60)–H(60)···Cl(9)		0.93	2.77	3.114(5)	103.4
C(61)–H(61)···Cl(7)_#3		0.93	2.78	3.505(5)	135.6
C(63)–H(63)···O(3)		0.93	2.33	2.814(5)	111.8
C(64)–H(64)···Cl(10)		0.93	2.60	2.995(5)	106.4
2					
C(3)–H(3)···Cl(2)_\$4		0.93	2.79	3.429(6)	126.4
C(3)–H(3)···O(1)_\$5		0.93	2.47	3.301(6)	148.2
C(12)–H(12)···O(2)		0.93	2.35	3.129(8)	140.8
C(25)–H(25)···Cl(2)		0.93	2.79	3.125(6)	102.8
C(28)–H(28)···O(1)		0.93	2.37	2.773(6)	105.8
C(29)–H(29)···Cl(3)		0.93	2.67	3.079(5)	107.1
3					
C(5)–H(5)···O(1)_\$6		0.93	2.47	3.279(5)	146.1
C(12)–H(12)···O(2)		0.93	2.34	3.127(4)	142.6
C(16)–H(16)···Cl(2)_\$7		0.93	2.75	3.514(4)	139.9
C(28)–H(28)···O(1)		0.93	2.18	2.860(4)	129.1
4					
C(5)–H(5)···O(1)_\$8		0.93	2.54	3.346(9)	145.0
C(12)–H(12)···O(2)		0.93	2.21	3.016(11)	145.0
C(28)–H(28)···O(1)		0.93	2.30	2.824(10)	115.3

#1: $-1 + x, y, z$; #2: $x, 1 + y, z$; #3: $2 - x, 1 - y, 1 - z$; #4: $1/2 - x, -y, -1/2 + z$; #5: $1 - x, -y, 1 - z$; #6: $1 - x, 1 - y, 1 - z$; #7: $1 + x, y, z$; #8: $2 - x, 2 - y, 1 - z$.

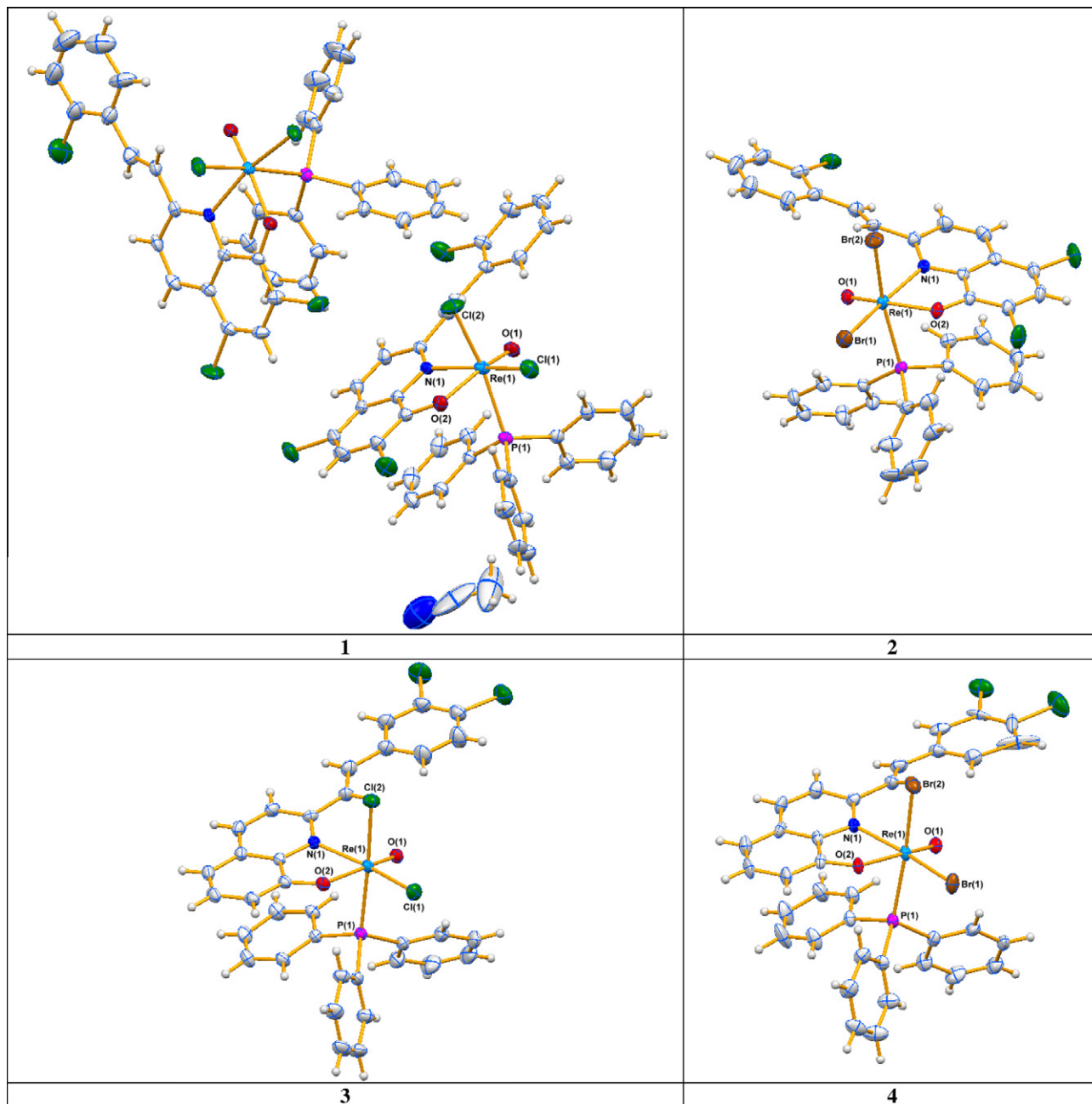


Fig. 1. The asymmetric units of **1**, **2**, **3** and **4**. Displacement ellipsoids are drawn at 50% probability.

3. Results and discussion

3.1. Preparation and infrared spectra

The styrylquinolines (5,7-dichloro-2-[2-(2-chlorophenyl)vinyl]quinolin-8-ol (HL₁) and 2-[2-(3,4-dichlorophenyl)vinyl]quinoline-8-ol (HL₂)) were prepared in high yields according to well-known method based on the condensation of 8-hydroxyquinaldine with appropriate aldehyde in acetic acid anhydride [20]. The purity and structures of HL₁ and HL₂ were determined by means of HPLC, NMR and mass spectroscopy (Supplementary materials).

The complexes [ReOCl₂(L₁)(PPh₃)₂·MeCN (**1**), [ReOBr₂(L₁)(PPh₃)₂] (**2**), [ReOCl₂(L₂)(PPh₃)₂] (**3**) and [ReOBr₂(L₂)(PPh₃)₂] (**4**) were obtained by ligand exchange reactions starting from [ReOX₃(PPh₃)₂] complexes and HL (Scheme 2). They were isolated as a dark green microcrystalline solids, moderately soluble in common

organic solvents. They show high stability toward air and moisture both in the solid state and in solution for several weeks at ambient temperature.

The IR spectra of **1–4** were characterized by strong absorptions at 974 cm⁻¹ for **1**, 972 cm⁻¹ for **2**, 965 cm⁻¹ for **3** and 968 cm⁻¹ for **4**, assigned to the Re=O stretching frequencies. These values are in the range typical of neutral six-coordinate monooxorhenium(V) complexes with an anionic phenolate oxygen coordinated *trans* to the oxo group [32]. A relatively high wavenumber of $\nu(\text{Re}=\text{O})$ suggests that the Re–hydroxy bond *trans* to the oxo ligand does not compete effectively for the Re_d orbitals. The absorptions in the region 1630–1540 cm⁻¹ were assigned to the $\nu(\text{C}=\text{N})$ modes of the chelating ligands [33].

The ¹H NMR spectra of **1–4** in DMSO-d₆ also confirm the presence of the chelating N,O-donor ligand and triphenylphosphine molecule in the coordination spheres of pseudo-octahedral Re(V)

Table 3The experimental and optimized bond lengths (Å) and angles (°) for **1** and **3**.

Bond lengths	1		3		Bond angles	1		3	
	Experimental	Optimized	Experimental	Optimized		Experimental	Optimized	Experimental	Optimized
Re(1)–O(1)	1.665(3)	1.679	1.675(2)	1.682	O(1)–Re(1)–O(2)	160.88(14)	159.88	162.99(11)	160.14
Re(1)–O(2)	2.020(3)	2.034	1.975(2)	2.018	O(1)–Re(1)–N(1)	92.03(14)	91.34	91.81(11)	91.62
Re(1)–N(1)	2.177(4)	2.204	2.188(3)	2.206	O(2)–Re(1)–N(1)	75.38(13)	75.01	75.80(10)	75.22
Re(1)–Cl(1)	2.3283(12)	2.398	2.3401(9)	2.404	O(1)–Re(1)–Cl(1)	101.73(11)	103.60	103.48(8)	103.94
Re(1)–Cl(2)	2.3703(12)	2.437	2.4041(9)	2.444	O(2)–Re(1)–Cl(1)	92.11(10)	91.32	89.65(7)	90.67
Re(1)–P(1)	2.4831(11)	2.559	2.4814(9)	2.558	N(1)–Re(1)–Cl(1)	165.78(10)	164.56	164.54(8)	163.95
					O(1)–Re(1)–Cl(2)	103.85(11)	102.13	98.00(9)	101.18
					O(2)–Re(1)–Cl(2)	89.59(9)	91.32	92.59(7)	92.35
					N(1)–Re(1)–Cl(2)	85.09(9)	84.25	85.14(7)	84.18
					Cl(1)–Re(1)–Cl(2)	88.12(5)	88.74	90.40(3)	88.89
					O(1)–Re(1)–P(1)	85.44(10)	85.70	84.48(9)	85.21
					O(2)–Re(1)–P(1)	81.07(8)	81.32	84.64(7)	81.76
					N(1)–Re(1)–P(1)	93.37(9)	96.45	93.28(7)	96.86
					Cl(1)–Re(1)–P(1)	91.29(4)	88.66	90.49(3)	88.47
					Cl(2)–Re(1)–P(1)	170.62(5)	172.13	177.09(3)	173.51
Re(2)–O(3)	1.660(3)				O(3)–Re(2)–O(4)	162.56(13)			
Re(2)–O(4)	1.999(3)				O(3)–Re(2)–N(2)	92.04(13)			
Re(2)–N(2)	2.184(3)				O(4)–Re(2)–N(2)	75.12(12)			
Re(2)–Cl(6)	2.3258(11)				O(3)–Re(2)–Cl(6)	102.85(10)			
Re(2)–Cl(7)	2.3859(12)				O(4)–Re(2)–Cl(6)	90.66(8)			
Re(2)–P(2)	2.4797(12)				N(2)–Re(2)–Cl(6)	164.99(10)			
					O(3)–Re(2)–Cl(7)	101.16(11)			
					O(4)–Re(2)–Cl(7)	90.20(9)			
					N(2)–Re(2)–Cl(7)	87.50(9)			
					Cl(6)–Re(2)–Cl(7)	87.76(4)			
					O(3)–Re(2)–P(2)	85.58(11)			
					O(4)–Re(2)–P(2)	83.71(9)			
					N(2)–Re(2)–P(2)	94.31(9)			
					Cl(6)–Re(2)–P(2)	88.79(4)			
					Cl(7)–Re(2)–P(2)	172.96(4)			

Table 4The experimental bond lengths (Å) and angles (°) for **2** and **4**.

Bond lengths	2		4		Bond angles	2		4	
	Experimental	Optimized	Experimental	Optimized		Experimental	Optimized	Experimental	Optimized
Re(1)–O(1)	1.665(4)		1.683(5)		O(1)–Re(1)–O(2)	159.55(15)		162.4(2)	
Re(1)–O(2)	2.014(3)		1.980(5)		O(1)–Re(1)–N(1)	89.35(15)		91.2(2)	
Re(1)–N(1)	2.196(4)		2.205(6)		O(2)–Re(1)–N(1)	75.00(14)		75.4(2)	
Re(1)–Br(1)	2.4764(6)		2.4777(9)		O(1)–Re(1)–Br(1)	100.57(11)		102.54(19)	
Re(1)–Br(2)	2.4978(15)		2.486(2)		O(2)–Re(1)–Br(1)	96.20(10)		91.54(15)	
Re(1)–P(1)	2.5251(7)		2.5451(9)		N(1)–Re(1)–Br(1)	169.28(10)		166.13(15)	
					O(1)–Re(1)–P(1)	88.78(14)		85.60(19)	
					O(2)–Re(1)–P(1)	80.03(11)		83.87(15)	
					N(1)–Re(1)–P(1)	95.97(12)		93.53(16)	
					Br(1)–Re(1)–P(1)	88.37(4)		89.77(5)	
					O(1)–Re(1)–Br(2)	102.86(14)		100.08(18)	
					O(2)–Re(1)–Br(2)	89.22(11)		90.39(15)	
					N(1)–Re(1)–Br(2)	85.65(12)		85.45(15)	
					Br(1)–Re(1)–Br(2)	88.15(2)		89.92(3)	
					P(1)–Re(1)–Br(2)	168.28(3)		174.24(5)	

Table 5Atomic charges from the natural population analysis (NPA) for [ReOCl₂(L₁)(PPh₃)] and [ReOCl₂(L₂)(PPh₃)].

Atom	Charge	
	[ReOCl ₂ (L ₁)(PPh ₃)]	[ReOCl ₂ (L ₂)(PPh ₃)]
Re(1)	+0.272	+0.276
O(1)	–0.334	–0.340
O(2)	–0.607	–0.610
N(1)	–0.409	–0.404
P(1)	+1.523	+1.519
Cl(1)	–0.214	–0.224
Cl(2)	–0.266	–0.279

atom. For **1** and **2** the protons of PPh₃ appear as multiplet in the range 7.65–7.50 ppm, which obscure some protons of the chelate

ligand. Triphenylphosphine protons of **3** and **4** exhibit as two multiplets in range 7.37–7.19 ppm. Unfortunately, complexes **1–4** exhibit limited solubility in most common solvents which prevented the recording of meaningful ¹³C NMR spectra.

3.2. Crystal structures

A definite proof for the structures of **1–4** is provided by the X-ray diffraction results. The crystallographic data of **1–4** are summarized in Table 1.

The intra- and intermolecular contacts [34,35] detected in the structures **1–4** are collected in Table 2. The structures **1–4** are stabilized by some C–H···O and C–H···X short contacts classified as weak hydrogen bonds. The classical hydrogen bonds are not found in **1–4**.

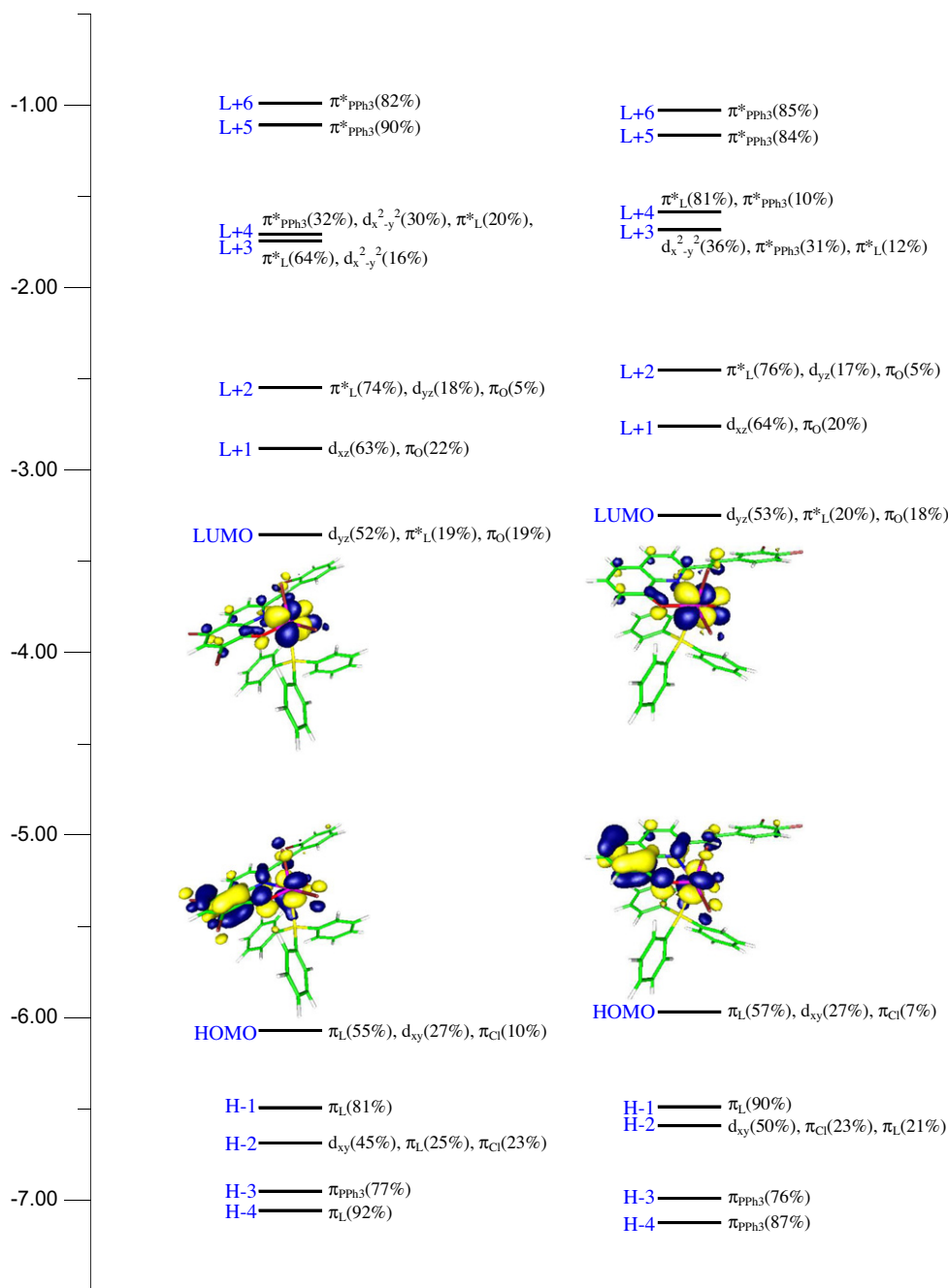


Fig. 2. The energy (eV), character and some contours of the unoccupied molecular orbitals of [ReOCl₂(L₁)(PPh₃)] and [ReOCl₂(L₂)(PPh₃)]. Positive values of the orbital contour are represented in blue (0.04 au) and negative values – in yellow (–0.04 au) (colour online).

The perspective drawings of the asymmetric units of **1–4** are presented in Fig. 1, and the selected bond distances and angles are collected in Tables 3 and 4.

All complexes show octahedral geometry about the rhenium atom defined by the terminal oxo-group, two halide ions in *cis* arrangement, the phosphorus of PPh₃ molecule, and the bidentate N,O donors of the L ligand. The multiple bonding ligand (terminal oxo) and narrow bite angle of the chelating ligand contribute to clear distortions of the pseudooctahedral environment of Re center in the [ReOX₂(HL_n)(PPh₃)] complexes. The high concentration of electronic density along the Re–O axis strongly influences the positions of the adjacent halogen atoms, which are pushed away. In all reported compounds, the oxygen donor of L is located *trans* to the

terminal oxo group. This is due to a strong *trans*-influence of the oxo group, forcing the harder oxygen atom of the N–O ligand into *trans* position. Such stereochemistry is well documented in the literature and seems to be the most common structure type for [ReOX₂(N–O)(PPh₃)] complexes.

The Re–O_t bond lengths of **1–4** fall in the range 1.639–1.760 Å, typical of mononuclear complexes of rhenium(V) having [ReO]³⁺ core, and indicate the presence of a triple bond Re≡O [36]. The interatomic distances between the rhenium atom and the oxygen atom of L ligand are somewhat shorter than an ideal single Re–O bond length. The single Re–O bond, predicted by the use of Pauling's covalent radius for oxygen and Cotton and Lippard's value for the octahedral covalent radius of rhenium(V), is equal *ca.*

Table 6The occupancy of the calculated natural bond orbitals (NBOs) between the rhenium and the oxo ligand for [ReOCl₂(L₁)(PPh₃)] and [ReOCl₂(L₂)(PPh₃)].

BD	Occupancy	Composition of NBO	BD*	Occupancy
<i>[ReOCl₂(L₁)(PPh₃)]</i>				
Re(1)–O(1)	1.99	0.561 (d) _{Re} + 0.828 (p) _O	0.828 (d) _{Re} – 0.561 (p) _O	0.22
Re(1)–O(1)	1.98	0.573 (d) _{Re} + 0.819 (p) _O	0.819 (d) _{Re} – 0.573 (p) _O	0.23
<i>[ReOCl₂(L₂)(PPh₃)]</i>				
Re(1)–O(1)	1.99	0.563 (d) _{Re} + 0.827 (p) _O	0.827 (d) _{Re} – 0.563 (p) _O	0.22
Re(1)–O(1)	1.98	0.574 (d) _{Re} + 0.819 (p) _O	0.819 (d) _{Re} – 0.574 (p) _O	0.24

BD denotes 2-center bond.

* Denotes antibond NBO.

Table 7Stabilization energies associated with delocalisation from the lone pair orbitals of the terminal oxo ligand for [ReOCl₂(L₁)(PPh₃)] and [ReOCl₂(L₂)(PPh₃)].

Donor orbital	Occupancy of donor orbital	Acceptor orbital	ΔE _{ij} (kcal/mol)
<i>[ReOCl₂(L₁)(PPh₃)]</i>			
(sp ^{0.82}) _{O(1)}	1.91	LP*(2)Re(1) [(sp ^{0.29} d ^{1.37}) _{Re(1)}]	12.07
		LP*(3)Re(1) [(sp ^{2.96} d ^{0.39}) _{Re(1)}]	17.72
		LP*(4)Re(1) [(p) _{Re(1)}]	51.17
		RY*(1)Re(1) [(d) _{Re(1)}]	10.34
(sp ^{1.83}) _{O(1)}	1.58	LP*(2)Re(1) [(sp ^{0.29} d ^{1.37}) _{Re(1)}]	183.87
		LP*(3)Re(1) [(sp ^{2.96} d ^{0.39}) _{Re(1)}]	24.45
		LP*(4)Re(1) [(p) _{Re(1)}]	52.13
<i>[ReOCl₂(L₂)(PPh₃)]</i>			
(sp ^{0.84}) _{O(1)}	1.91	LP*(2)Re(1) [(sp ^{0.30} d ^{1.39}) _{Re(1)}]	11.59
		LP*(3)Re(1) [(sp ^{2.88} d ^{0.39}) _{Re(1)}]	17.68
		LP*(4)Re(1) [(p) _{Re(1)}]	50.25
		RY*(1)Re(1) [(d) _{Re(1)}]	10.42
(sp ^{1.79}) _{O(1)}	1.59	LP*(2)Re(1) [(sp ^{0.30} d ^{1.39}) _{Re(1)}]	182.35
		LP*(3)Re(1) [(sp ^{2.88} d ^{0.39}) _{Re(1)}]	25.55
		LP*(4)Re(1) [(p) _{Re(1)}]	51.63

Table 8The energy and molar absorption coefficients of experimental absorption bands and the electronic transitions calculated with the TDDFT method for [ReOCl₂(L₁)(PPh₃)].

State	Excitations	E _{cal} (eV)	λ _{cal} (nm)	×c4 _{cal}	λ _{expt} (nm)	Character
S ₁	H→L	1.61	769.8	0.0114	634.4	π(L)/d/π(Cl)→d/π*(L)
S ₃	H→2→L	2.33	532.5	0.0349		d/π(L)/π(Cl)→d/π*(L)
S ₄	H→1→L	2.61	475.1	0.1332	448.2	π(L)→d/π*(L)
S ₆	H→L+2	2.90	427.6	0.0927		π(L)/d/π(Cl)/π(PPh ₃)→π*(L)/d
S ₁₅	H→1→L+2	3.35	370.6	0.1726		π(L)→π*(L)/d
S ₁₇	H→2→L+2	3.50	354.2	0.2171	356.1	d/π(L)/π(Cl)→π*(L)/d
S ₂₁	H→10→L	3.66	338.4	0.0637		π(L)→d/π*(L)
S ₂₂	H→11→L	3.67	337.7	0.0642		π(Cl)→d/π*(L)
	H→10→L					π(L)→d/π*(L)
S ₂₅	H→L+4	3.81	325.9	0.2610	330.5	π(L)/d/π(Cl)→π*(PPh ₃)/d/π*(L)
S ₂₆	H→8→L+1	3.82	325.0	0.0760		π(PPh ₃)→d
S ₄₂	H→2→L+4	4.37	283.7	0.0728		d/π(L)/π(Cl)→π*(PPh ₃)/d/π*(L)
	H→2→L+3					d/π(L)/π(Cl)→π*(L)/d
S ₅₀	H→3→L+3	4.61	269.2	0.0907		π(PPh ₃)→π*(L)/d
	H→3→L+4					π(PPh ₃)→π*(PPh ₃)/d/π*(L)
S ₆₀	H→7→L+3	4.83	256.7	0.0627		π(PPh ₃)/π(Cl)→π*(L)/d
	H→7→L+4					π(PPh ₃)/π(Cl)→π*(PPh ₃)/d/π*(L)
S ₁₀₇	H→5→L+6	5.45	227.7	0.0505	222.3	π(L)/d→π*(PPh ₃)
S ₁₀₈	H→7→L+5	5.47	226.8	0.0552		π(PPh ₃)/π(Cl)→π*(PPh ₃)
S ₁₁₅	H→3→L+7	5.56	222.8	0.0425		π(PPh ₃)→π*(L)
	H→8→L+5					π(PPh ₃)→π*(PPh ₃)
					207.6	

ε – Molar absorption coefficient (dm³ mol⁻¹ cm⁻¹); f – oscillator strength; H – highest occupied molecular orbital; L – lowest unoccupied molecular orbital.

2.04 Å [37]. It indicates only small delocalization of electron density in the O=Re–O unit in these compounds and seems to be typical feature of *cis*-X₂X isomers of [ReOCl₂(N–O)(PPh₃)] with an anionic phenolate oxygen coordinated *trans* to the oxo group.

The Re(1)–X(1) distances *trans* to the phosphorus atom of PPh₃ molecule are slightly longer than the Re(1)–X(2) bonds *trans* to the nitrogen atom of the HL_n ligand. It indicates structural *trans* effect of the PPh₃ ligand.

Table 9The energy and molar absorption coefficients of experimental absorption bands and the electronic transitions calculated with the TDDFT method for [ReOCl₂(L₂)(PPh₃)].

State	Excitations	E_{cal} (eV)	λ_{cal} (nm)	$\times c_{\text{cal}}$	λ_{expt} (nm)	Character
S ₁	H→L	1.63	762.9	0.0123	636.6	$\pi(\text{L})/d/\pi(\text{Cl})\rightarrow d/\pi^*(\text{L})$
S ₃	H-2→L	2.33	531.8	0.0310		$d/\pi(\text{Cl})/\pi(\text{L})\rightarrow d/\pi^*(\text{L})$
S ₄	H-1→L	2.68	463.4	0.0578	432.2	$\pi(\text{L})\rightarrow d/\pi^*(\text{L})$
	H-2→L+1					$d/\pi(\text{Cl})/\pi(\text{L})\rightarrow d$
S ₅	H-1→L	2.71	456.9	0.0805	312.2	$\pi(\text{L})\rightarrow d/\pi^*(\text{L})$
S ₆	H→L+2	2.91	425.8	0.1679		$\pi(\text{L})/d/\pi(\text{Cl})/\pi(\text{PPh}_3)\rightarrow \pi^*(\text{L})/d$
S ₁₃	H-2→L+2	3.41	363.4	0.0865	312.2	$d/\pi(\text{Cl})/\pi(\text{L})\rightarrow \pi^*(\text{L})/d$
	H-1→L+2					$\pi(\text{L})\rightarrow \pi^*(\text{L})/d$
S ₁₆	H-1→L+2	3.55	349.4	0.4268	251.0	$\pi(\text{L})\rightarrow \pi^*(\text{L})/d$
	H-2→L+2					$d/\pi(\text{Cl})/\pi(\text{L})\rightarrow \pi^*(\text{L})/d$
S ₂₀	H-10→L	3.75	330.2	0.1371	205.4	$\pi(\text{L})\rightarrow d/\pi^*(\text{L})$
S ₂₄	H→L+4	3.86	321.4	0.1325		$\pi(\text{L})/d/\pi(\text{Cl})\rightarrow \pi^*(\text{L})/\pi^*(\text{PPh}_3)$
S ₂₅	H→L+4	3.87	320.6	0.2782	$\pi(\text{L})/d/\pi(\text{Cl})\rightarrow \pi^*(\text{L})/\pi^*(\text{PPh}_3)$	
S ₄₅	H-1→L+4	4.44	279.0	0.0593	251.0	$\pi(\text{L})\rightarrow \pi^*(\text{L})/\pi^*(\text{PPh}_3)$
S ₅₂	H→L+7	4.69	264.2	0.0685		$\pi(\text{L})/d/\pi(\text{Cl})\rightarrow \pi^*(\text{L})$
S ₅₃	H-3→L+3	4.70	264.0	0.1306	205.4	$\pi(\text{PPh}_3)\rightarrow d/\pi^*(\text{PPh}_3)/\pi^*(\text{L})$
S ₆₄	H-6→L+3	4.93	251.7	0.0289		$\pi(\text{PPh}_3)/\pi(\text{Cl})\rightarrow d/\pi^*(\text{PPh}_3)/\pi^*(\text{L})$
S ₈₄	H-7→L+3	5.23	237.2	0.0423	205.4	$\pi(\text{L})\rightarrow d/\pi^*(\text{PPh}_3)/\pi^*(\text{L})$
S ₉₆	H-3→L+6	5.37	231.0	0.0367		$\pi(\text{PPh}_3)\rightarrow \pi^*(\text{PPh}_3)$
S ₁₀₆	H-6→L+5	5.47	226.8	0.0655	205.4	$\pi(\text{PPh}_3)/\pi(\text{Cl})\rightarrow \pi^*(\text{PPh}_3)$
S ₁₀₇	H-9→L+4	5.49	225.7	0.0597		$\pi(\text{PPh}_3)\rightarrow \pi^*(\text{L})/\pi^*(\text{PPh}_3)$
S ₁₁₈	H-15→L+2	5.69	218.1	0.0390	205.4	$\pi(\text{Cl})/\pi(\text{L})\rightarrow \pi^*(\text{L})/d$
	H-11→L+4					$\pi(\text{Cl})\rightarrow \pi^*(\text{L})/\pi^*(\text{PPh}_3)$

ϵ – Molar absorption coefficient ($\text{dm}^3 \text{mol}^{-1} \text{cm}^{-1}$); f – oscillator strength; H – highest occupied molecular orbital; L – lowest unoccupied molecular orbital.

3.3. Geometry optimization, charge distribution, electronic structure, NBO analysis

The DFT calculations have been performed to get an insight in the electronic structures and explain bonding nature and spectral properties of the complexes [ReOCl₂(L₁)(PPh₃)] and [ReOCl₂(L₂)(PPh₃)]. Before the calculations of the electronic structures of the studied compounds, their geometries were optimized in singlet states using the DFT method with the B3LYP functional. The optimized geometric parameters of [ReOCl₂(L₁)(PPh₃)] and [ReOCl₂(L₂)(PPh₃)] are given in Table 3.

In general, the predicted bond lengths and angles are in agreement with the values based upon the X-ray crystal structure data, and the general trends observed in the experimental data are well reproduced in the calculations. The B3LYP method in combination with the LANL2DZ basis gives an excellent estimation of Re–O_t bond length with deviation of +0.014 Å for [ReOCl₂(L₁)(PPh₃)] and +0.007 Å for [ReOCl₂(L₂)(PPh₃)]. The Re–N and other Re–O distances are also well reproduced (deviations of the distances Re–N are equal to 0.026 and 0.018 Å for **1** and **3**, and deviations of the Re–O bond lengths are 0.014 for **1** and 0.043 Å for **3**). Larger deviations are noticed for Re–Cl and Re–P bond lengths, but they are also satisfactory for this level of theory.

Table 5 presents the atomic charges from the natural population analysis (NPA) for **1** and **3**. The calculated charges on the rhenium atoms in **1** and **3** are considerably lower than the formal charge of +5, and the populations of the d_{xy} , d_{xz} , d_{yz} , $d_{x^2-y^2}$ and d_{z^2} orbitals of the central atoms are following: 1.097, 0.941, 1.271, 0.825 and 1.376 for **1** and 1.119, 0.951, 1.098, 0.840 and 1.502 for **3**. It confirms significant charge donation from the ligands. The P atom is positively charged, and the charges on the terminal oxo, chloride and oxygen atom of L are significantly smaller than –2, –1 and –1, respectively. The terminal oxo ions are less negative in comparison with the oxygen atoms of L ligand. It indicates the higher electron density delocalization from the terminal ligands towards the rhenium centres and corresponds to differences in the Re–O(1) and Re–O(2) bond lengths.

The complexes [ReOCl₂(L₁)(PPh₃)] and [ReOCl₂(L₂)(PPh₃)] are closed-shell structures. Their partial molecular orbital diagrams with several HOMO and LUMO contours are presented in Fig. 2. For both complexes under study the HOMO–LUMO gaps equal to 2.72 eV. The HOMO and HOMO-2 of [ReOCl₂(L₁)(PPh₃)] and [ReOCl₂(L₂)(PPh₃)] are composed of rhenium d_{xy} and p chloride orbitals in antibonding arrangement to metal orbital as well as contain admixture from L ligand orbitals. HOMO–1 and some lower-energy occupied MOs of **1** and **3** correspond to orbitals of the chelate ligand or PPh₃. The LUMO and LUMO+1 of **1** and **3** are predominately localized on the rhenium atom (d_{xz} and d_{yz} orbitals) with some contribution of p_{π} oxygen orbitals and π^* -antibonding orbitals of ligand L. To large extent these orbitals can be ascribed as π -antibonding rhenium–oxygen molecular orbitals. The LUMO+3 and LUMO+4 orbitals of [ReOCl₂(L₁)(PPh₃)] and LUMO+3 of [ReOCl₂(L₂)(PPh₃)] are contributed by metal orbitals $d_{x^2-y^2}$. Higher-energy unoccupied MOs have $\pi^*(\text{PPh}_3)$ and $\pi^*(\text{L})$ character. Larger number of electron-withdrawing halide substituents in ligand L₁ in comparison with L₂ exerts an influence on energy level of frontier orbitals of [ReOCl₂(L₁)(PPh₃)] and [ReOCl₂(L₂)(PPh₃)]. Ligand L₁ decreases energy level of the highest occupied and the lowest unoccupied MOs in relation to complex **2**.

For further understanding of the bond characteristics in reported complexes [ReOCl₂(L₁)(PPh₃)] and [ReOCl₂(L₂)(PPh₃)], natural bond orbital (NBO) studies have been performed. Table 6 presents the occupancies and hybridization of the calculated natural bond orbitals (NBOs) between the rhenium and the oxo ligands. Table 7 shows the occupancies and atomic orbital compositions of the lone pairs (LP) of the oxo ligands, as well as the character of the acceptor orbital and stabilization energies (ΔE_{ij}) for the corresponding donor–acceptor interactions for [ReOCl₂(L₁)(PPh₃)] and [ReOCl₂(L₂)(PPh₃)]. For both complexes the results of NBO point to the existence of two Re–O_t natural bond orbitals, which result from overlapping of the empty d_{xy} and d_{yz} rhenium orbitals with the occupied p_x and p_z orbitals of terminal oxo ligand. Therefore they are of π character. Lack of $\sigma_{\text{Re-O}_t}$ natural orbital indicates a conceivable predominant Coulomb-type Re–ligand interaction

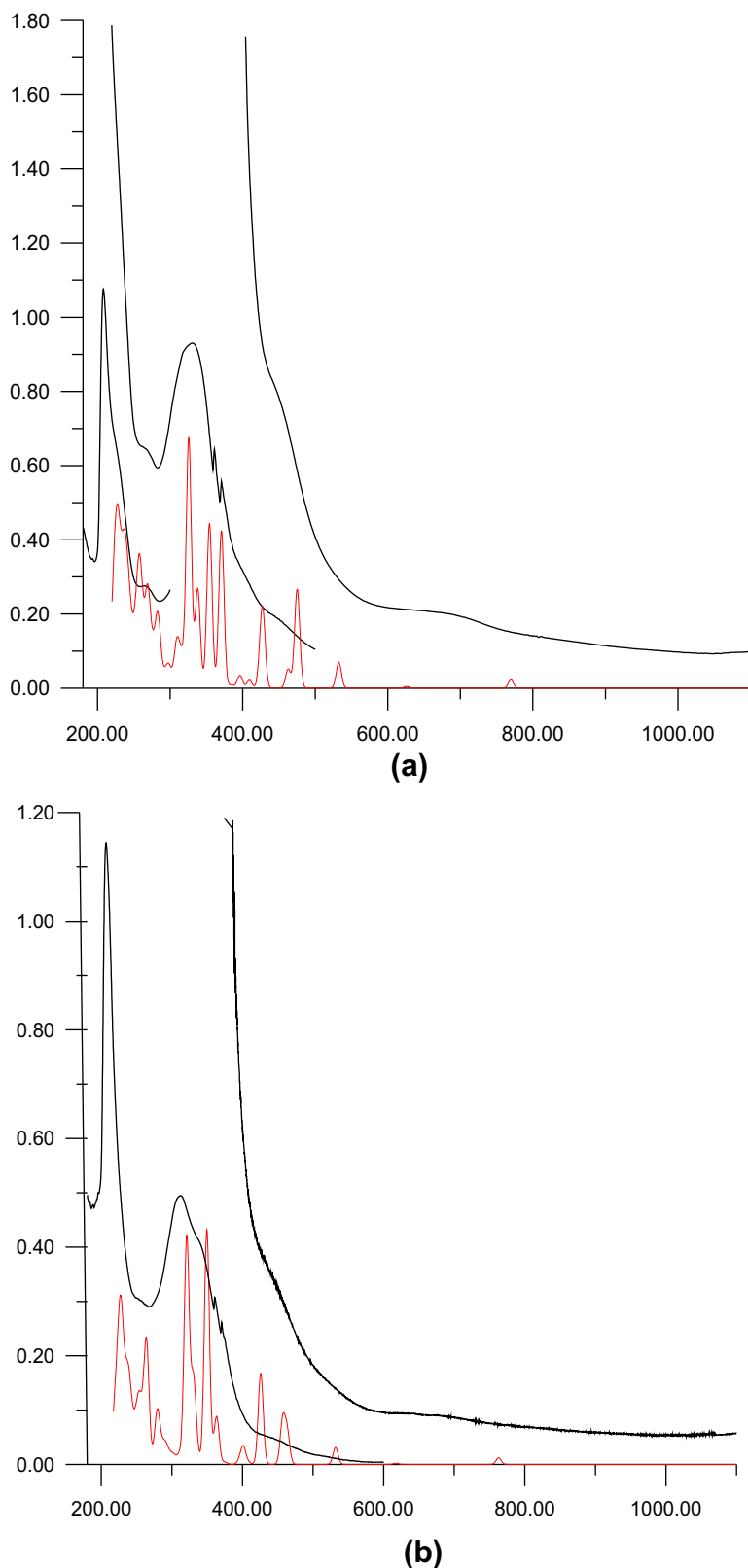


Fig. 3. The experimental (black) and calculated (red) electronic absorption spectra of [ReOCl₂(L₁)(PPh₃)] (a) and [ReOCl₂(L₂)(PPh₃)] (b) (colour online).

[38]. The terminal oxo ligand of [ReOCl₂(L₁)(PPh₃)] and [ReOCl₂(L₂)(PPh₃)] has two lone pair orbitals, and electron density from one of them is strongly delocalized into non-Lewis rhenium orbital

(see Table 8). The nature of Re–O_t bonds is in agreement with the results obtained in previous works regarding analysis of the bonding nature of rhenium(V) oxocomplexes [39].

3.4. Electronic spectra

The energies and characters of the selected singlet excited states for complexes **1** and **3** are listed in Tables 8 and 9, together with experimental data. The energy of each excited is vertical excitation energy in eV from the ground state and for the high energy part of the spectrum only excited states with the greatest oscillator strengths are displayed in Tables 8 and 9. Assignment of the character of each excited state was based on the compositions of the occupied and virtual MOs of the dominant configuration(s) for that excited state. The experimental and calculated results are also graphically compared in Fig. 3, presenting the experimental and calculated electronic absorption spectra of **1** and **3**. In Fig. 3 each calculated transition is represented by a gaussian function $y = ce^{-bx^2}$ with the height (c) equal to the oscillator strength and b equal to 0.04 nm^{-2} .

As shown in Fig. 3, the studied complexes have very similar absorption character and TDDFT calculations well correlate with the experimental absorptions. The longest wavelength experimental bands at 634.4 nm for **1** and 636.6 nm for **3** originate from the excitations between HOMO or HOMO–2 and the lowest unoccupied MO. As it can be seen from the Fig. 2, the highest occupied molecular orbital of **1** and **3** are composed of d_{xy} rhenium atomic orbital, p chloride orbitals and π orbitals of the chelate ligand, the lowest occupied molecular orbital of **1** and **3** are delocalized on central ion and π -antibonding orbitals of the N–O ligand. Accordingly, the transitions at 634.4 and 636.6 nm can be seen as delocalized MLLCT (*metal–ligand-to–ligand CT*) transitions. For bromide rhenium complexes these transitions are red-shifted and occur at 672.2 nm for **2** and 658.2 nm for **4**.

The absorption bands with maxima at 448.2 and 356.1 nm for **1** and 432.2 and 312.2 nm for **3** are attributed to *ligand–metal charge transfer* $\pi(\pi(\text{Cl})/\pi(\text{L})\rightarrow\text{d})$ and *ligand–ligand charge transfer* transitions. The transitions leading to the intense bands in high energy region of **1** and **3** are mainly of *ligand–ligand charge transfer* (LLCT) and intraligand (IL) character.

4. Conclusions

5,7-Dichloro-2-[2-(2-chlorophenyl)vinyl]quinolin-8-ol (HL₁) and 2-[2-(3,4-dichlorophenyl)vinyl]quinoline-8-ol (HL₂) react with [ReOX₃(PPh₃)₂] (X = Cl, Br) to give [ReOCl₂(L₁)(PPh₃)₂].MeCN (**1**), [ReOBr₂(L₁)(PPh₃)₂] (**2**), [ReOCl₂(L₂)(PPh₃)₂] (**3**) and [ReOBr₂(L₂)(PPh₃)₂] (**4**). The complexes have been characterized structurally and spectroscopically. The L₁ and L₂ ligands coordinate in a chelate way via N- and O-donor atoms, and the oxygen donor of the chelate ligand is located *trans* to the terminal oxo (O_t) group due to a strong *trans*-influence of O_t ligand. The O=Re–O core with multiply bonded oxo ligand is stabilized to some extent due to accessible π -donation from rhenium to PPh₃ molecule adopting *cis* position with respect to the linear O=Re–O unit. The X-ray studies and NBO analysis confirm a triple bond between the rhenium and the terminal oxo ligand. DFT and TD-DFT calculations applied to **1** and **3** resulted in appropriate prediction of the UV–Vis spectra and enabled a detailed assignment of the electronic transitions to the experimental absorptions. For both complexes the longest wavelength experimental bands can be seen as MLLCT (*metal–ligand-to–ligand CT*) transitions, which is a consequence of delocalized character of molecular orbitals involved in the electronic transitions.

Acknowledgements

This work was financed by the Polish National Science Centre (NCN), under Grant No. 2011/03/N/ST5/04522. W. Cieslik was

supported by a DoktorIS fellowship. The GAUSSIAN09 calculations were carried out in the Wrocław Centre for Networking and Supercomputing, WCSS, Wrocław, Poland. Grant No. 18.

Appendix A. Supplementary material

CCDC 905844, 905845, 905846, 905847 contains the supplementary crystallographic data for C₇₂H₅₁N₃O₄Cl₁₀P₂Re₂ (**1**), C₃₅H₂₄NO₂PCl₃Br₂Re (**2**), C₃₅H₂₅Cl₄NO₂PRe (**3**), C₃₅H₂₅Br₂Cl₂NO₂PRe (**4**). These data can be obtained free of charge via <http://www.ccdc.cam.ac.uk/conts/retrieving.html>, or from the Cambridge Crystallographic Data Centre, 12 Union Road, Cambridge CB2 1EZ, UK; fax: +44 1223-336-033; or e-mail: deposit@ccdc.cam.ac.uk. Supplementary data associated with this article can be found, in the online version, at <http://dx.doi.org/10.1016/j.poly.2012.12.028>.

References

- [1] R. Musiol, M. Serda, S. Hensel-Bielowka, J. Polanski, *Curr. Med. Chem.* 17 (2010) 1960.
- [2] C.R. Harris, A. Thorarensen, *Curr. Med. Chem.* 11 (2004) 2213.
- [3] J. Jampilek, R. Musiol, M. Pesko, K. Kralova, M. Vejsova, J. Carroll, A. Coffey, J. Finster, D. Tabak, H. Niedbala, V. Kozik, J. Polanski, J. Csolle, J. Dohnal, *Molecules* 14 (2009) 1145.
- [4] S. Vangapandu, M. Jain, R. Jain, S. Kaur, P.P. Singh, *Bioorg. Med. Chem.* 12 (2004) 2501.
- [5] K. Andries, P. Verhasselt, J. Guillemont, H.W. Gohlmann, J.M. Neefs, H. Winkler, J. Van Gestel, M. Zhu, E. Lee, P. Williams, D. de Chaffoy, E. Huitric, S. Hoffner, E. Cambau, C. Truffot-Pernot, N. Lounis, V. Jarlier, *Science* 307 (2005) 223.
- [6] J. Vinsova, A. Imramovsky, J. Jampilek, J. Monreal-Ferriz, M. Dolezal, *Med. Chem.* 7 (2008) 12.
- [7] R. Musiol, J. Jampilek, J.E. Nycz, M. Pesko, J. Carroll, K. Kralova, M. Vejsova, J. O'Mahony, A. Coffey, A. Mrozek, J. Polanski, *Molecules* 15 (2010) 288.
- [8] R. Musiol, D. Tabak, H. Niedbala, B. Podeszwa, J. Jampilek, K. Kralova, J. Dohnal, J. Finster, A. Mencil, J. Polanski, *Bioorg. Med. Chem.* 16 (2008) 4490.
- [9] R. Musiol, J. Jampilek, K. Kralova, D.R. Richardson, B. Kalinowski, B. Podeszwa, J. Finster, H. Niedbala, A. Palka, J. Polanski, *Bioorg. Med. Chem.* 15 (2007) 1280.
- [10] A. Mrozek-Wilczkiewicz, D.S. Kalinowski, R. Musiol, J. Finster, A. Szurko, K. Serafin, S.K. Kamalapuram, Z. Kovacevic, J. Jampilek, A. Ratuszna, J. Rzeszowska-Wolny, D.R. Richardson, J. Polanski, *Bioorg. Med. Chem.* 18 (2010) 2664.
- [11] M. Serda, D. Kalinowski, A. Mrozek-Wilczkiewicz, R. Musiol, A. Szurko, A. Ratuszna, N. Pantarat, Z. Kovacevic, A.M. Merlot, D.R. Richardson, J. Polanski, *Bioorg. Med. Chem. Lett.*, in press.
- [12] J. Polanski, H. Niedbala, R. Musiol, D. Tabak, B. Podeszwa, R. Gieleciak, A. Bak, A. Palka, T. Magdziarz, *Acta Pol. Pharm. Drug Res.* 61 (2004) 3.
- [13] S.S. Jurisson, J.D. Lydon, *Chem. Rev.* 99 (1999) 2205.
- [14] S. Liu, D.S. Edwards, *Chem. Rev.* 99 (1999) 2235.
- [15] E.S. Mull, V.J. Sattigeri, A.L. Rodriguez, J.A. Katzenellenbogen, *Bioorg. Med. Chem.* 10 (2002) 1381.
- [16] P. Blower, *Dalton Trans.* (2006) 1705.
- [17] J. Gancheff, C. Kremer, E. Kremer, O.N. Ventura, *J. Mol. Struct. (Theochem.)* 580 (2002) 107.
- [18] E. Reed, L.A. Curtiss, F. Weinhold, *Chem. Rev.* 88 (1988) 899.
- [19] G. Rouschias, G. Wilkinson, *J. Chem. Soc. A* (1966) 465.
- [20] R. Musiol, B. Podeszwa, J. Finster, H. Niedbala, J. Polanski, *Monatsh. Chem.* 137 (2006) 1211.
- [21] Oxford Diffraction, CrysAlis PRO, Oxford Diffraction Ltd., Yarnton, England, 2011.
- [22] G.M. Sheldrick, *SHELXS-97*, Program for Crystal Structure Resolution, Univ. of Göttingen, Göttingen, Germany, 1997.
- [23] G.M. Sheldrick, *SHELXL-97*, Program for Crystal Structures Analysis, Univ. of Göttingen, Göttingen, Germany, 1997.
- [24] M.J. Frisch, G.W. Trucks, H.B. Schlegel, G.E. Scuseria, M.A. Robb, J.R. Cheeseman, G. Scalmani, V. Barone, B. Mennucci, G.A. Petersson, H. Nakatsuji, M. Caricato, X. Li, H.P. Hratchian, A.F. Izmaylov, J. Bloino, G. Zheng, J.L. Sonnenberg, M. Hada, M. Ehara, K. Toyota, R. Fukuda, J. Hasegawa, M. Ishida, T. Nakajima, Y. Honda, O. Kitao, H. Nakai, T. Vreven, J.A. Montgomery, J.E. Peralta, F. Ogliaro, M. Bearpark, J.J. Heyd, E. Brothers, K.N. Kudin, V.N. Staroverov, R. Kobayashi, J. Normand, K. Raghavachari, A. Rendell, J.C. Burant, S.S. Iyengar, J. Tomasi, M. Cossi, N. Rega, J.M. Millam, M. Klene, J.E. Knox, J.B. Cross, V. Bakken, C. Adamo, J. Jaramillo, R. Gomperts, R.E. Stratmann, O. Yazyev, A.J. Austin, R. Cammi, C. Pomelli, J.W. Ochterski, R.L. Martin, K. Morokuma, V.G. Zakrzewski, G.A. Voth, P. Salvador, J.J. Dannenberg, S. Dapprich, A.D. Daniels, O. Farkas, J.B. Foresman, J.V. Ortiz, J. Cioslowski, D.J. Fox, *GAUSSIAN 09*, Revision A.1, Gaussian, Inc., Wallingford, CT, 2009.
- [25] A.D. Becke, *J. Chem. Phys.* 98 (1993) 5648.
- [26] C. Lee, W. Yang, R.G. Parr, *Phys. Rev. B* 37 (1988) 785.
- [27] P.J. Hay, W.R. Wadt, *J. Chem. Phys.* 82 (1985) 299.

- [28] K. Eichkorn, F. Weigend, O. Treutler, R. Ahlrichs, *Theor. Chem. Acc.* 97 (1997) 119.
- [29] P.M.W. Gill, B.G. Johnson, J.A. Pople, M.J. Frisch, *Chem. Phys. Lett.* 197 (1992) 499.
- [30] M.E. Casida, J.M. Seminario (Eds.), *Recent Developments and Applications in Modern Density Functional Theory, Theoretical and Computational Chemistry*, vol. 4, Elsevier, Amsterdam, 1996.
- [31] E.D. Glendening, A.E. Reed, J.E. Carpenter, F. Weinhold, *NBO Version 3.1*.
- [32] U. Mazzi, F. Refosco, F. Tisato, G. Bandoli, M. Nicolini, *J. Chem. Soc., Dalton Trans.* (1986) 1623.
- [33] K. Nakamoto, *Infrared and Raman Spectra of Inorganic and Coordination Compounds*, fourth ed., Wiley-Interscience, New York, 1986.
- [34] G.A. Jeffrey, W. Saenger, *Hydrogen Bonding in Biological Structures*, Springer-Verlag, 1994.
- [35] G.R. Desiraju, T. Steiner, *The Weak Hydrogen Bond in Structural Chemistry and Biology*, Oxford University Press, 1999.
- [36] J.M. Mayer, *Inorg. Chem.* 27 (1988) 3899.
- [37] S.R. Flechter, A.C. Skapski, *J. Chem. Soc., Dalton Trans.* (1972) 1073.
- [38] M.L. Kuznetsov, A.J.L. Pombeiro, *J. Chem. Soc., Dalton Trans.* (2003) 738.
- [39] B. Machura, M. Wolff, J. Kusz, R. Kruszynski, *Polyhedron* 28 (2009) 2949.